J. Fluid Mech. (1989), *vol.* 201, *pp.* 99–121
Printed in Great Britain

Pulsating flow over an ellipse at an angle of attack

By D. S. MATHIOULAKIS AND D. P. TELIONIS
Department of Engineering Science & Mechanics, Virginia Polytechnic Institute & State University, Blacksburg, VA 20461, USA

(Received 3 June 1987 and in revised form 11 August 1988)

Two-component LDV measurements are obtained over an ellipse at an angle of attack. Detailed information is provided for the stagnation region, the two separation regions and the two free shear layers. Steady and unsteady flow measurements are presented. Periodic disturbances in the oncoming stream are introduced and ensemble-averaged unsteady data are obtained. An integral picture of laminar flow over a lifting body with no sharp edges is thus presented, which is readily available for comparison with asymptotic or numerical calculations.

1. Introduction

For many decades, the problem of separation was studied from a steady-flow viewpoint. In analytical studies the steady-flow equations were solved. In experimental studies, mean flow measurements were obtained. Yet, in real life, steady separation hardly exists. Moreover, small disturbances of the free stream quite often excite spectacular periodic activities in the wake of bluff bodies.

Moore (1958), Rott (1956) and Sears (1956) identified the significance of unsteady separation. Numerical and experimental efforts followed, as discussed in extensive reviews (Sears & Telionis 1975; Shen 1978; Telionis 1979, 1981). The past decade has seen impressive analytical advances on laminar separation (Smith 1977, 1979, 1985*a*; Messiter 1979, 1983; Sychev 1979). For the first time, the global characteristics of the flow field were tied together with the local behaviour of separation, yet only local unsteady effects, as for example hydrodynamic instabilities, were accounted for by such asymptotic studies (Smith 1985*b*, 1986).

For symmetric two-dimensional bluff bodies, free shear layer interaction gives rise to a well-organized undulation, which soon generates large coherent vortical structures. The activity induces considerable fluctuations of the locations of separation. Thus, with steady far-field conditions, the flow organizes itself into well-structured periodic motions which influence significantly the entire field, including separation and stagnation. The situation is different for slender bodies like airfoils at an angle of attack. For high enough angles of attack, the free shear layer emanating from the leading edge of the airfoil develops for some distance over a solid surface, the suction side of the airfoil. The interaction with the shear layer released at the trailing edge is initiated further downstream. The behaviour is very similar to the effect of a splitter plate positioned downstream of a circular cylinder. There again, vortex formation is suppressed but only until the end of the splitter plate. With vortex shedding activities displaced further downstream, separation is very little affected by periodicity in the wake. It is this situation we examine in the present paper, for steady flow first and subsequently extended to unsteady flow.

The work reported in this paper is a continuation of an experimental effort on

unsteady laminar separation. In earlier reports (Telionis & Mathioulakis 1984; Mathioulakis & Telionis 1985, 1987), we discuss the problem of laminar separation over a curved surface with particular attention to the immediate neighbourhood of separation. In these references the reader will also find an extensive list and brief discussion of earlier contributions. In the present paper we report on an extension of our work to include detailed measurements near, upstream and downstream of separation, as well as beyond the tail of the body, into the wake. The data presented here therefore offer a detailed picture of unsteady separating flow over a bluff body. These data are readily available for comparison with numerical calculations.

Work on this problem has been conducted in the same facility for quite a few years. In our earlier efforts we employed a one-channel laser-Doppler velocimeter (LDV). Disturbances were introduced in the flow either locally (Telionis & Koromilas 1978; Koromilas & Telionis 1980) or in the free stream (Mathioulakis & Telionis 1985, 1987). In the latter cases, the tunnel speed was fluctuating uniformly about a mean and the model was held still. The data acquisition system has been recently expanded and fully computerized. A two-component LDV system is employed (Mathioulakis & Telionis 1987) and data are obtained and processed on line by a laboratory computer.

Most of the early contributions on unsteady laminar separation were conducted on simple geometrical configurations, inducing artificially adverse pressure gradients (Despard & Miller 1971; Didden & Ho 1985). Until now, all of the work of the present group as well was conducted on diffuser-type models, whereby a boundary layer is allowed to grow on the floor of the tunnel, or on suspended walls, to eliminate the effects of tunnel wall turbulence. The flow was then led over a backward-facing section which induced separation. In the present paper we study the flow over a bluff body, an ellipse at an angle of attack mounted in the middle of the tunnel. This shape was chosen because it lacks the dominating character of a sharp trailing edge. Moreover, it accepts convenient numerical and analytical simulation.

Good physical insight can be obtained by examining vorticity distributions. Experimentally, it has been almost impossible to measure directly vorticity. One of the main reasons has been the fact that the slightest drift in the reading of hot wires would reduce the accuracy of measuring velocity differences, as reported by Francis *et al.* (1979) and Didden & Ho (1985). LDV measurements are free of drifting and therefore are perfectly suited for measurement of vorticity. In the present paper we present conditionally averaged vorticity data, obtained by laser-Doppler velocimetry.

2. Facilities and instrumentation

The present experiments were conducted in the VPI water tunnel which is described in Telionis & Koromilas (1978), Koromilas & Telionis (1980) and Mezaris *et al.* (1987). Some recent significant modifications and improvements are discussed in Mathioulakis & Telionis (1987). These essentially are a disturbing system which generates an accurately controlled periodic variation in the tunnel speed and honeycomb-screen additions to reduce the turbulence level in the test section. The tunnel speed can be represented by

$$U_\infty = U_0 + A\cos(2\pi ft), \tag{1}$$

where U_0 is the mean speed, A is the amplitude of the pulsation and f is the frequency of a very nearly harmonic disturbance. The periodic variations range in amplitude

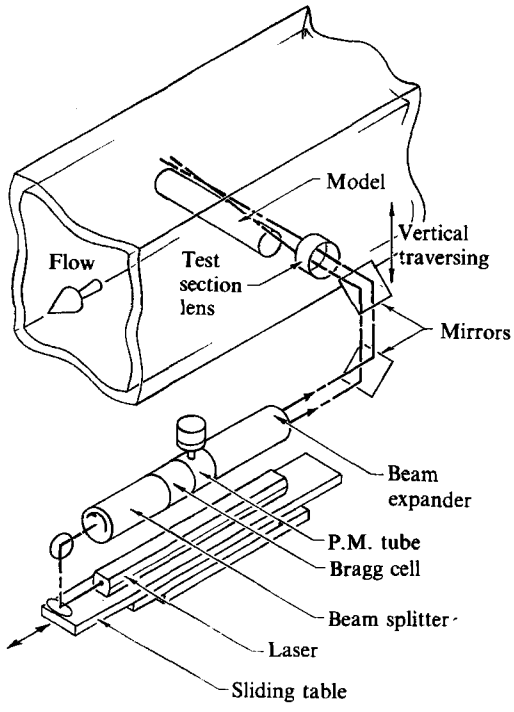

FIGURE 1. The LDV system in a backward-scattering mode, showing the traversing mirrors.

from 3% to 17% peak to peak and in frequency from 0.2 Hz to 6 Hz. The lowest turbulence level measured by an LDV was about 0.4%.

A two-channel LDV system was employed to measure simultaneously two orthogonal velocity components. Our system, shown schematically in figure 1, is essentially the same as that described in Mathioulakis & Telionis (1987). We use two sets of Bragg cells for shifting two of the three beams by 40 MHz and 60 MHz respectively. The beams are reflected over two sets of mirrors which provide accurate traversing in the vertical direction. Light is received in a backward-scattering mode. A single photo-multiplier is then used and the signal is down-mixed and filtered to provide instantaneous Doppler signals for two velocity components. The three beams entering the test section are arranged in such a way that the two velocity components measured are inclined by approximately 45° with respect to the predominant direction of the flow. The desired components are then calculated on-line by the laboratory computer.

In order to study the phenomenon of unsteady separation, a well-organized disturbance in the form of equation (1) was introduced in the oncoming stream via a rotating vane as described in Mathioulakis & Telionis (1987). The free stream was thus oscillated with a non-vanishing mean and the period of oscillation was fixed at 4.8 s. The tunnel velocity may slowly drift and on occasion within a few hours deviated by 3% from the original setting. To ensure uniformity, the free-stream velocity was monitored by a third LDV channel and all measurements were instantaneously normalized by this quantity.

The initiation of data acquisition was triggered by a pulse sent to the laboratory computer at a fixed opening of the rotating vane. The LDV signals were then

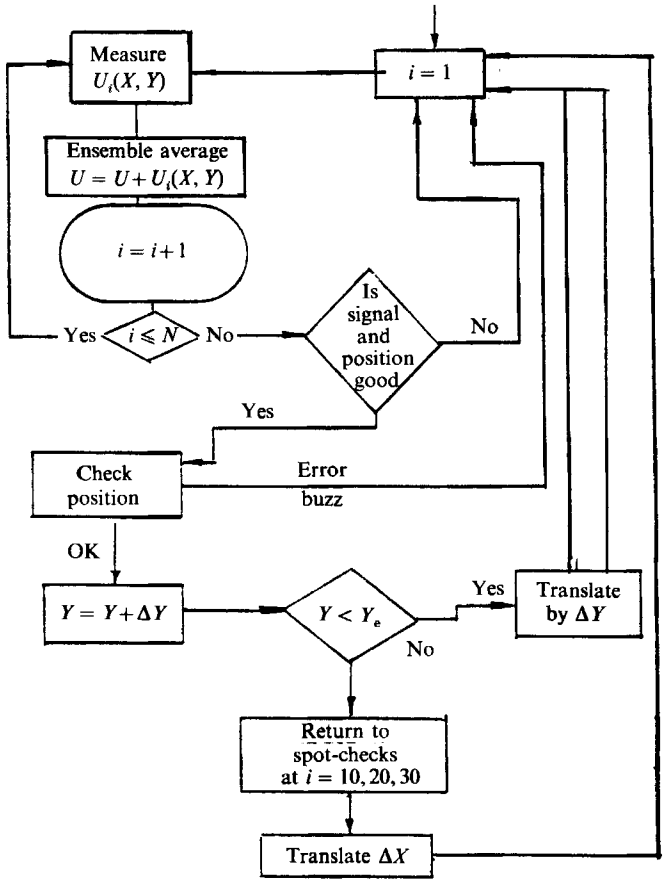

FIGURE 2. Flow chart for data acquisition.

conditionally averaged. For purposes of frequency domain analysis, 160 instantaneous values per period were stored. For the display of time-domain data only 16 points per period were stored. A flow chart of the data acquisition process is shown in figure 2.

The measurements at a particular station came to an end when the probe volume touched the surface of the model, which was accompanied by an abrupt increase of the signal noise level. In this way we were able to define the distance of the surface from the previous measuring point with an accuracy equal to the smallest displacement, which for this sequence of measurements was 0.125 mm, or 0.125 % of the model's chord length.

3. Description of the experiments

The two-dimensional flow field about an ellipse at an angle of attack was investigated with emphasis on five sections of the flow (figure 3), namely the front stagnation region, the two separation regions and the two free shear layers emanating from the separation points. Two sets of experiments were run, one with a steady and one with a periodically oscillating free stream.

The model was made of aluminium and had a major axis $2a = 100.1$ mm and a

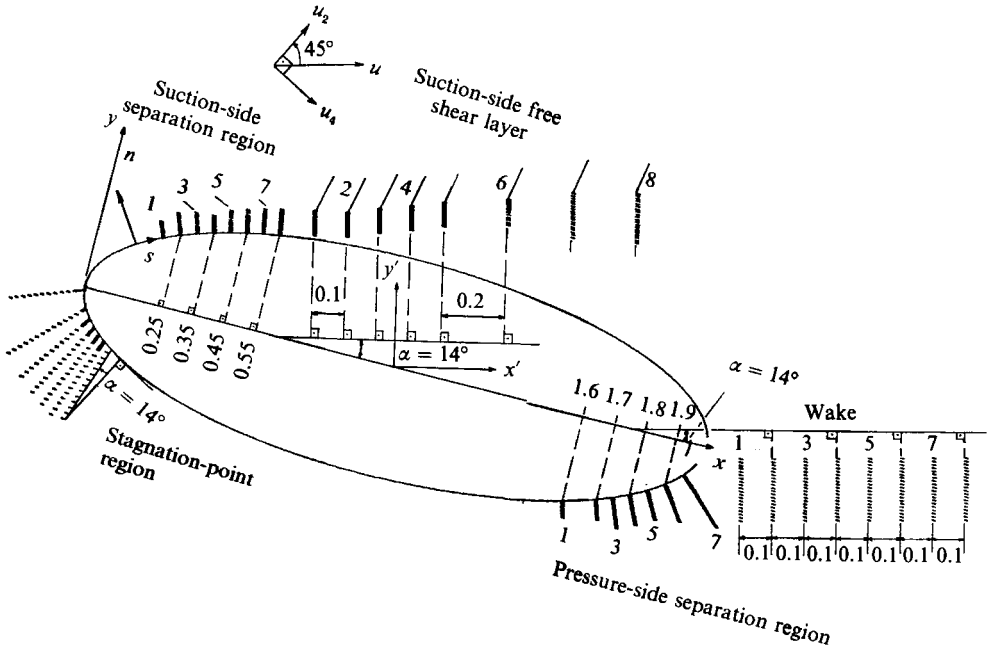

FIGURE 3. The coordinate systems and the measuring grid.

minor axis $2b = 33.75$ mm, giving an axes ratio of $a/b = 2.96$. This ratio was employed by Schubauer who conducted experiments on an ellipse about half a century ago. It was also chosen by a contemporary investigator (C.-M. Ho, University of Southern California, private communication) whose work is parallel to ours. Unfortunately the work of Schubauer was confined to a zero angle of attack and the data of Ho are not yet available. No comparison is therefore yet possible.

The model spanned the distance of 218 mm between two false tunnel walls and was free to rotate about its centre, facilitating the adjustment of the angle of attack, α, which was defined as the angle between the major axis and the free-stream velocity. In order to adjust this angle accurately, we followed a trial-and-error procedure as follows. As a tool of micropositioning we employed the traversing mechanism which displaces the LDV measuring volume as discussed earlier. Starting from a specific point far from the surface of the model, we moved the laser beams in a direction normal to the surface until they hit it. If the distance travelled by the beams was not equal to that calculated theoretically for the specific α, then the ellipse was given a small rotation about its spanwise axis. The procedure was repeated, until the distances travelled by the laser beams from several reference points to the surface of the model coincided with theoretical estimates of coordinates. The angle of attack was chosen to be 14°.

Two simultaneous velocity components were obtained by LDV. These are denoted by u_2 and u_4 as shown in figure 3. In the experiments described here, we employed an additional LDV system to record the variation of the free-stream velocity. This was an one-component LDV in the forward-scatter mode. It was positioned approximately 3 chord lengths upstream of the leading edge of the ellipse, and its output signal was fed to a TSI 1995 counter. The instantaneous free-stream velocity as well as the two velocity components obtained in the region close to the ellipse by

the two-component LDV system were stored in a minicomputer (MINK-11). The normalization of the velocity components by the instantaneous free-stream improved the quality of the data.

The velocity measurements were obtained in the midspan region of the elliptical cylinder in order to avoid the wall effects and their associated three-dimensional flow patterns. In the unsteady case the free-stream magnitude was varied sinusoidally in time, with a period of $T = 4.8$ s and a peak-to-peak amplitude of 10% normalized by the time-mean velocity, which was 14.3 cm/s. Therefore, the mean Reynolds number $Re_m = 2aU_\infty/\nu$ and the frequency parameter $2a\omega/U_\infty$ were 14300 and 0.91, respectively. There were 16 instantaneous values per period stored for each velocity component and the free stream. These data were ensemble averaged on line and only the phase-averaged values were stored. For every phase value ϕ or rather the corresponding time t_ϕ, the ensemble-averaged value of a velocity component was generated according to the formula

$$\hat{u}(x, y, t_\phi) = \frac{1}{N}\sum_1^N u_n(x, y, t_\phi) \tag{2}$$

where u_n represents a single realization.

4. Results and discussion

Measuring grids were defined within five regions. The coordinate system and the regions where measurements were concentrated are shown in figure 3. In the following, we discuss the velocity patterns in each of the five regions of the flow around the ellipse.

4.1. *Suction-side separation region*

Eight velocity profiles were obtained in the separating boundary layer on the suction side, namely at $x/a = 0.2$–0.55, where a is one half of the major axis of the ellipse. The distance $\Delta x/a$ between two adjacent stations was 0.05. At each station, the measuring volume was displaced normal to the model surface, with a smallest displacement of 0.125 mm, while the maximum number of data points per station was 33. The signals were conditionally averaged over 16 cycles. In figure 4 we show phase-averaged velocity vectors while in figure 5 we display the corresponding u- and v-components parallel and normal to the wall, respectively. In figure 5 the vertical axis is the distance n normal to the wall at the station of interest. The solid line corresponds to smoothed data obtained by a standard routine which fits locally second-degree polynomials to the experimental data.

The amplitude of the excursion of the point of zero skin friction is approximately only 5% of the major axis of the ellipse. A more pronounced periodic disturbance can be observed in deviations of the separation line and the locus of zero velocity from the wall. This can be most clearly seen by observing the thickness of the reverse-flow region in the most downstream stations.

The smoothed data were used for the calculation of phase-averaged vorticity contours of $\omega = \partial u/\partial y - \partial v/\partial x$, non-dimensionalized by U_∞/a. Vorticity contours are displayed in the frames of figure 6. In these figures both axes have been non-dimensionalized by the quantity a. These contours display a familiar peak on the wall upstream of the point at which a velocity inflectional profile, $\partial^2 u/\partial y^2 = 0$ appears at the wall. The point where $\partial^2 u/\partial y^2$ vanishes at the wall can be easily

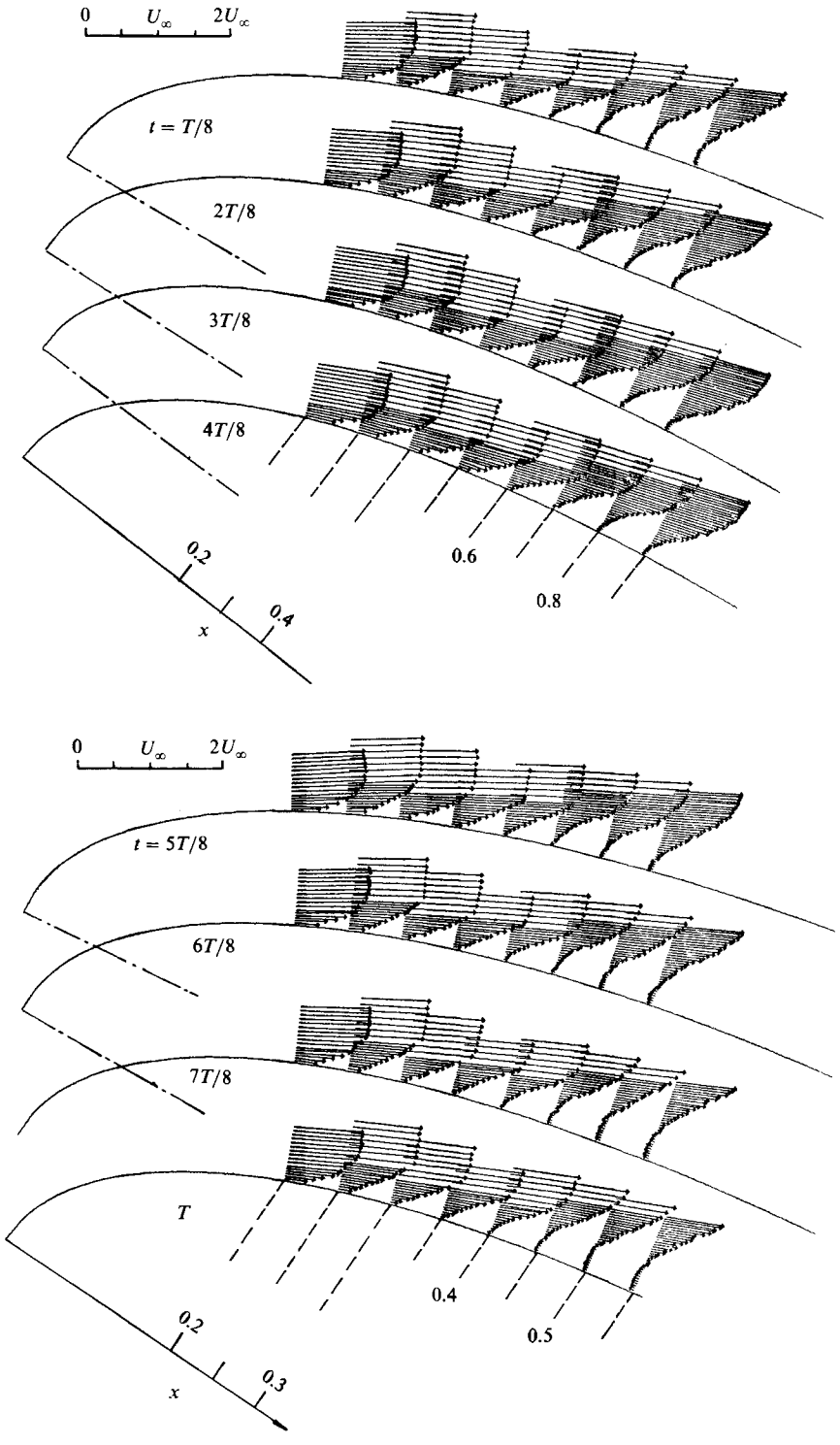

FIGURE 4. Suction-side separation. Velocity vectors at stations $x/a = 0.2, 0.25, 0.3, 0.35, 0.4, 0.45, 0.5, 0.55$ and at eight instances within one period.

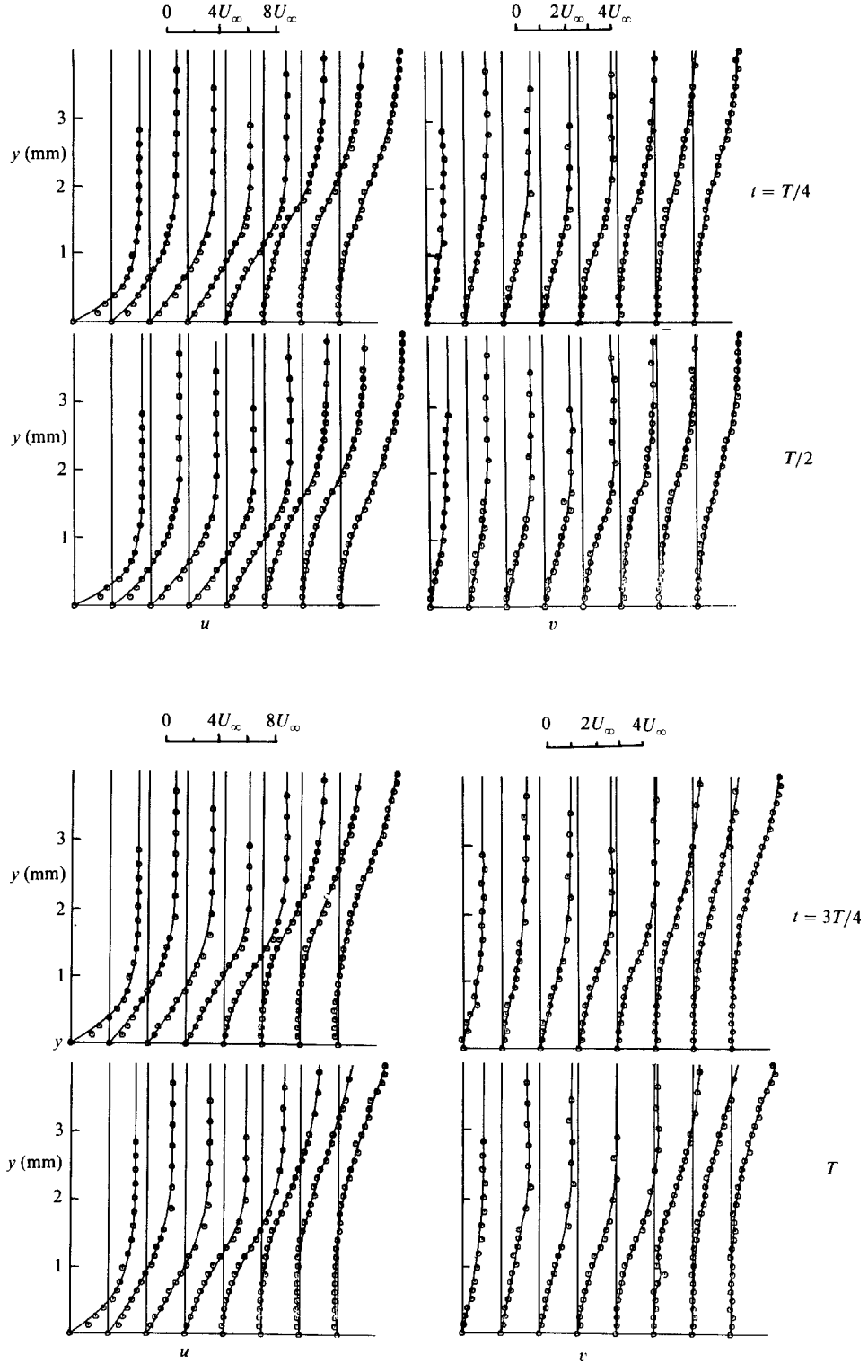

FIGURE 5. Velocity profiles (u, v) at suction-side separation region and four instances within a period.

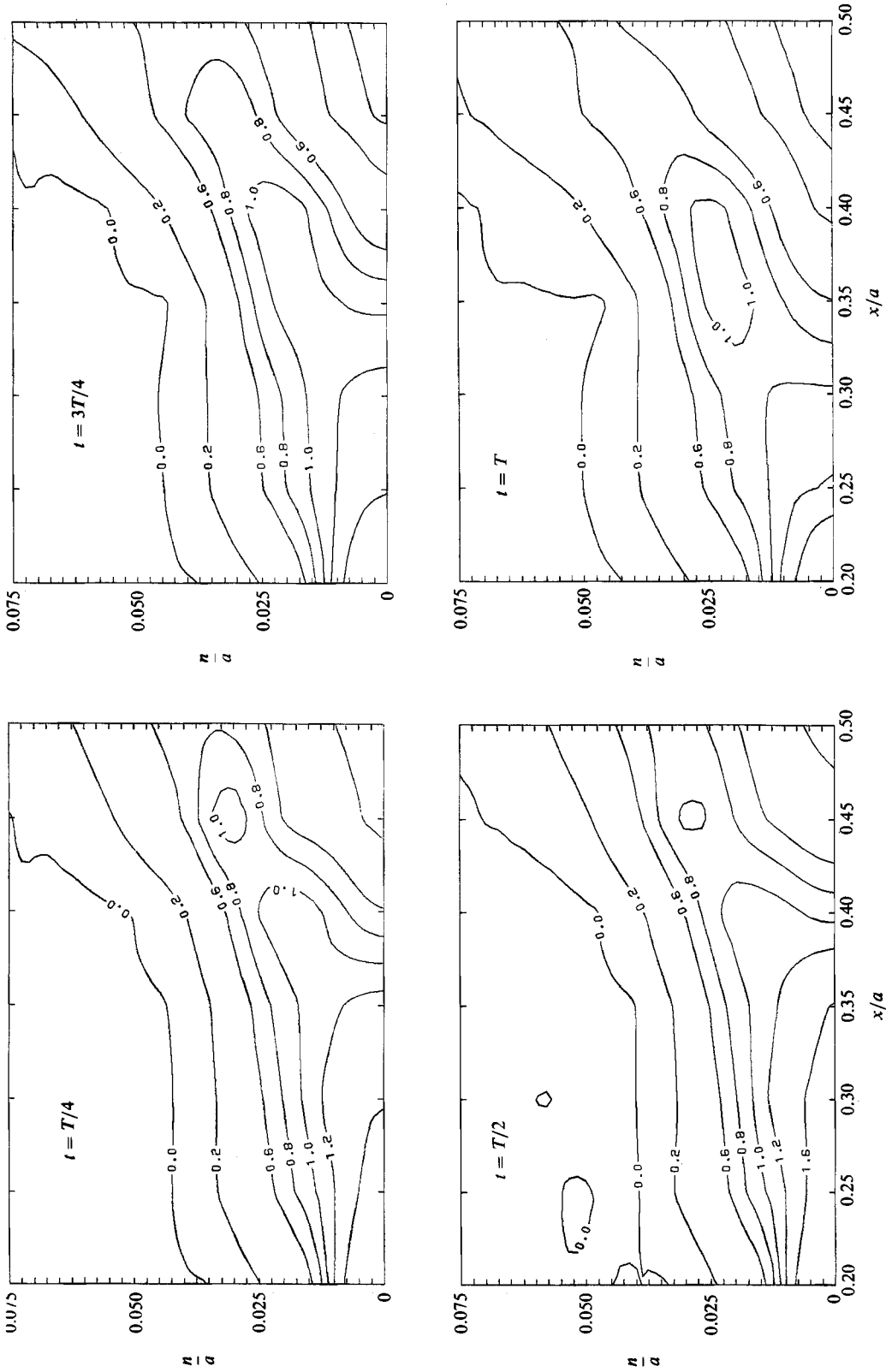

FIGURE 6. Vorticity contours at suction-side separation region and four phases within a period. Numerical values of $\omega/10$ are displayed on the contours.

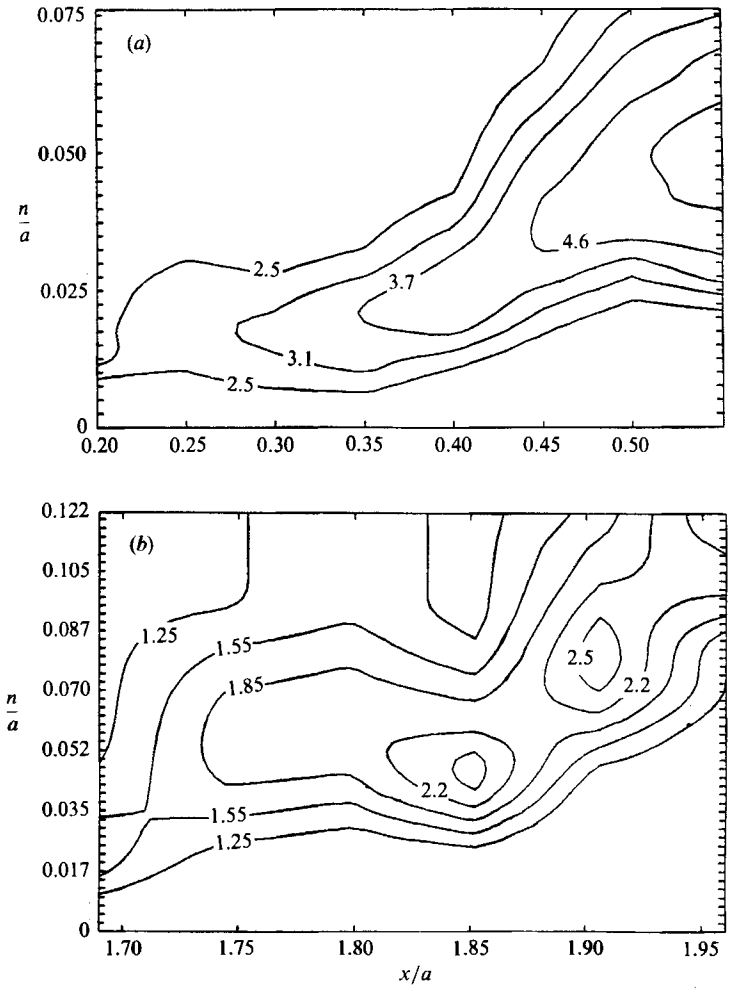

FIGURE 7. Amplitude contours at (*a*) suction-side separation region, (*b*) pressure-side separation region.

identified in the figures as the point where a vorticity contour meets the wall at a right angle. From then on, and as the free shear layer starts developing, the peak values in the vorticity distribution occur away from the wall. Significant here is the fact that certain 'islands' are formed and convected downstream in a periodic fashion. Shedding of vorticity is therefore implemented in increments. The phenomenon is locked to the external driving frequency.

In figure 7(*a*), the amplitudes of oscillation normalized by the free-stream amplitude are shown. The amplitude of the oscillation increases continuously beyond separation. For flows disturbed locally, Mezaris *et al.* (1987) found that the amplitudes peak near separation. This is not the case here for flows disturbed in the free stream.

An FFT analysis of the time-dependent u-component did not reveal any significant phase variation across the boundary layer. The driving frequency was clearly the most dominant frequency. A comparison between the steady and

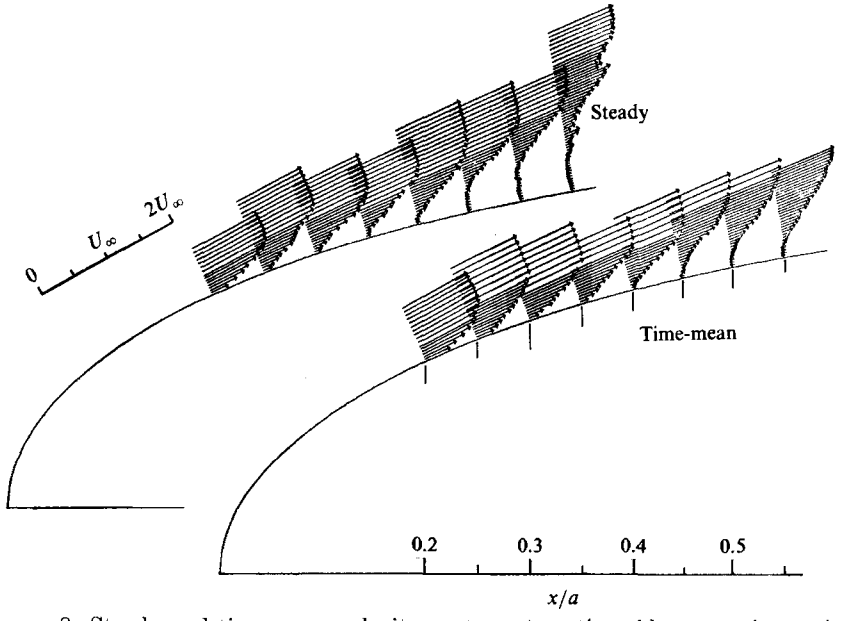

FIGURE 8. Steady and time-mean velocity vectors at suction-side separation region.

unsteady flow fields is possible by observing the frames in figure 8 where the steady and time-mean velocity vectors are shown.

Streamlines can be constructed by integrating the u-component of the velocity along the n-direction. This provides a check on the accuracy of the measurements, since the slope of these streamlines should match with the slope obtained by evaluating the ratio of the measured quantities v and u. This is essentially a check that the continuity equation is met by the two measured components of the velocity. A typical pattern of streamlines generated by integrating the n-component is displayed in figure 9.

The process of constructing streamlines by integrating the parallel component of the velocity is not very accurate here, because considerable variations may be encountered in the s-direction, especially as separation is approached. We feel that measuring directly the two components by the present method is a far more reliable method for the determination of the local direction of the flow.

The basic conclusions drawn by the analysis of the data in this region of the flow are the following:

(*a*) deceleration of the free stream results in a thickening of the reversed-flow region and a small upstream excursion of the zero-skin-friction point; the opposite happens when the flow accelerates;

(*b*) the amplitude of oscillation increases in the shear-layer region and in the downstream direction (maximum observed value: 5.8 times the free-stream amplitude);

(*c*) the zero-skin-friction point for the time-mean velocity field is located downstream of that for the steady case;

(*d*) the thickness of the reversed-flow region is considerably larger for steady than for the mean unsteady flow;

(*e*) for the chosen values of Reynolds number and reduced frequency, unsteadiness results in a small downstream displacement of the mean position of separation as well.

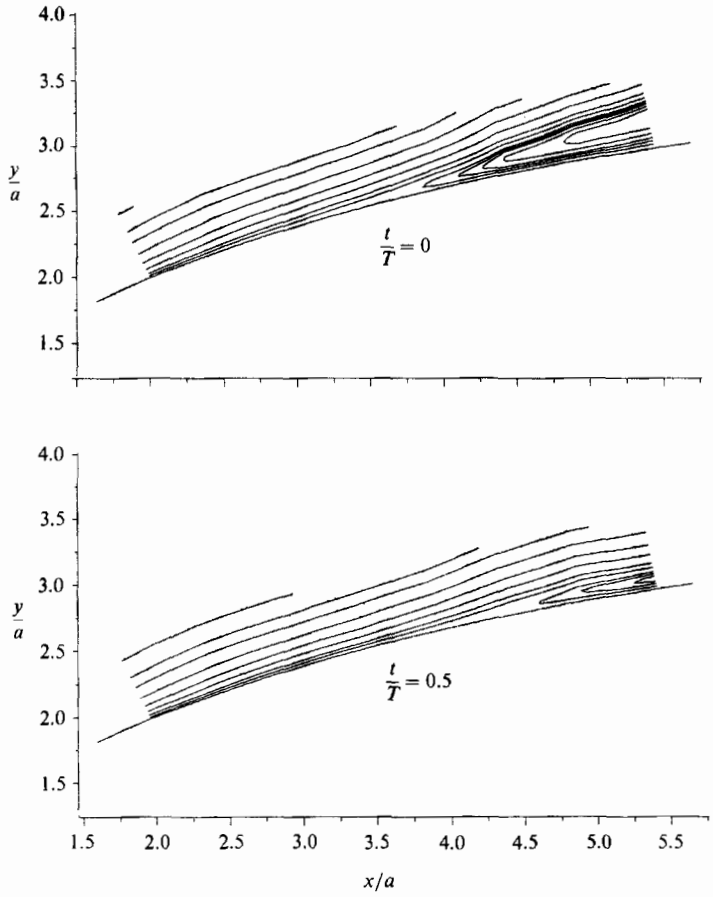

FIGURE 9. Streamlines on the suction side of the model.

4.2. *Suction-side free-shear layer*

Measurements in this area of the flow were obtained at eight stations (see figure 3). The distance between two adjacent points in a station was 0.2 mm except for stations 7 and 8 where it was 0.4 mm. The unsteady motion of this layer is shown in figure 10 where velocity vectors have been drawn at time intervals of $T/8$. The basic features of the flow in this region appear to be:

(*a*) increase of the velocity amplitude in the downstream direction;

(*b*) thickening of the reverse-flow region during deceleration of the oncoming velocity;

(*c*) in the farthest downstream stations, the velocity vectors appear to have random directions. This is an indication that turbulence has set in, and that the number of samples is quite insufficient to create converged values for the phase-averaged measurements;

(*d*) the width of the shear layer increases in the downstream direction, while its maximum vorticity values drop. This information can provide a measure of the effect of molecular diffusion.

In figure 11 the steady and unsteady time-mean vectors are shown. We notice that, in the mean, the shear layer is farther from the surface for the steady than the unsteady case. In other words, the wake is broader for steady flow.

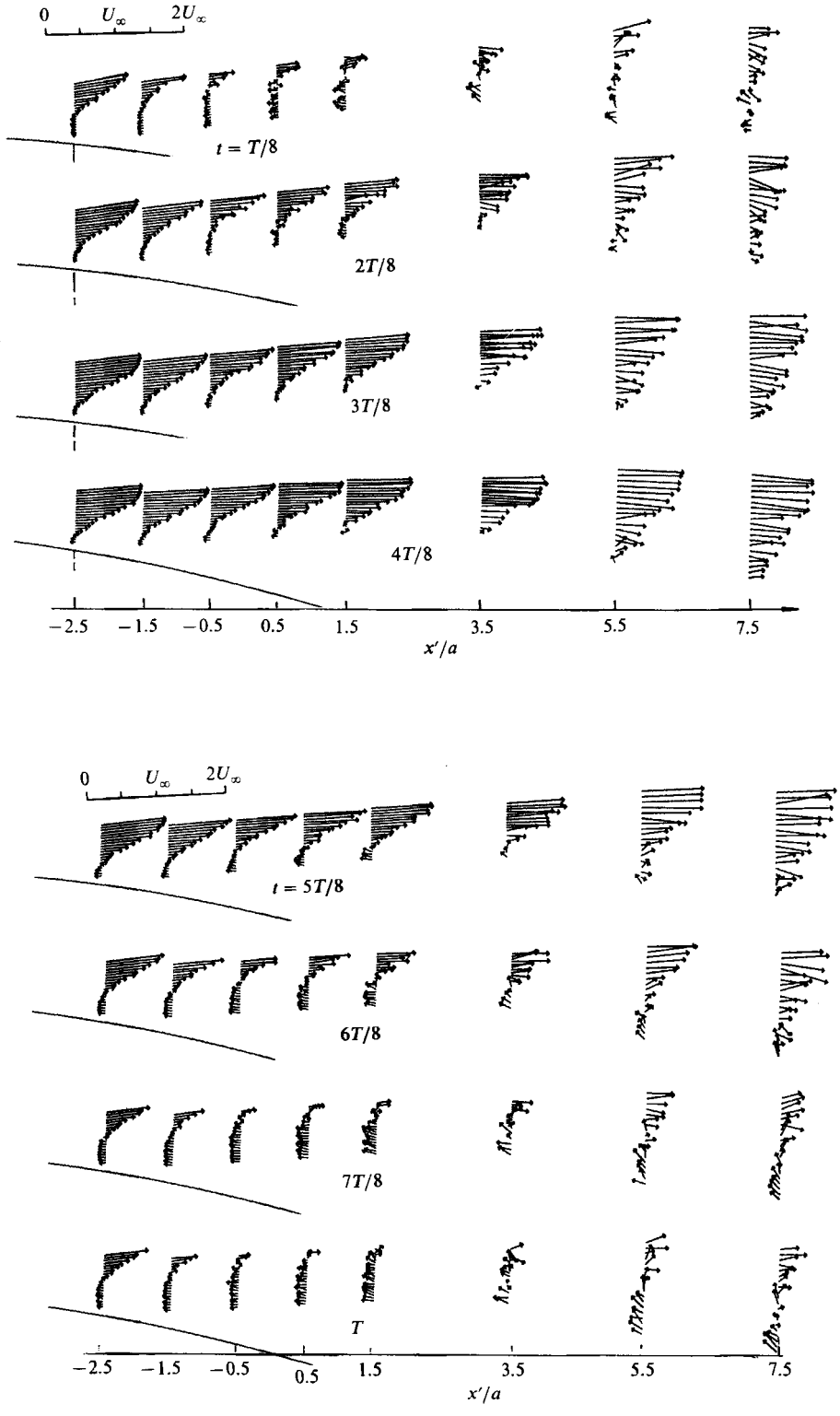

FIGURE 10. Velocity vectors at suction-side free shear layer at eight instances within one period.

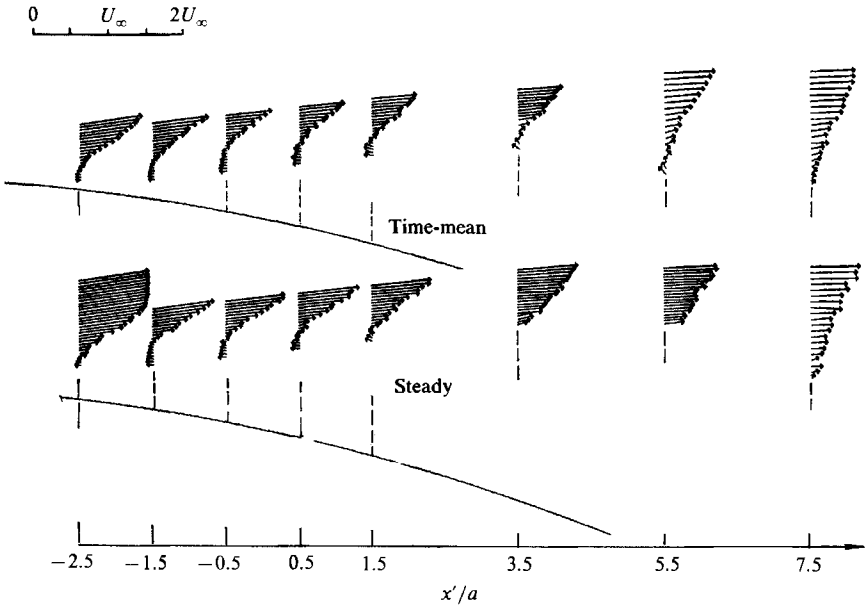

FIGURE 11. Steady and time-mean velocity vectors at suction-side free shear layer.

4.3. *Stagnation point*

The numerical prediction of the flow about a bluff body becomes easier if information about its stagnation point is available since the integration of the boundary-layer equations starts from this point. This information controls the circulation around the airfoil and therefore the instantaneous lift sustained by the body. Measurements in the stagnation-point region were obtained for the steady and unsteady case. In order to approach the surface of the model as closely as possible, we rotated the optical train so that the beams were located in space as shown in figure 12.

For the steady flow, we took measurements along eight stations normal to the surface and at points with x/a coordinates 0.02, 0.04, 0.06, 0.08, 0.10, 0.12, 0.14, 0.16, respectively. The velocity vectors are shown in figure 12. We notice that the flow has been decelerated significantly, since its magnitude is 60% of the free stream at a distance of $0.25a$ from the wall. The component parallel to the wall near stagnation varies linearly with distance from the stagnation point, in agreement with standard inviscid-flow stagnation theory. Apparently, boundary-layer measurements were impossible in this region because of its very small thickness. For the oscillating-free-stream case, velocities were obtained along seven stations not normal to the wall, as shown in figure 13. In this case the stagnation point appears to oscillate along the wall, moving downstream when the flow decelerates.

The main conclusions for the stagnation region are:

(*a*) the amplitude of oscillation increases when the surface is approached, with a maximum value of 2.5 times the free-stream amplitude obtained at the station closest to the x-axis (1st station);

(*b*) the steady-flow point of stagnation is approximately located at $x/a = 0.04$ and shifts in the mean to $x/a = 0.05$ for unsteady flow.

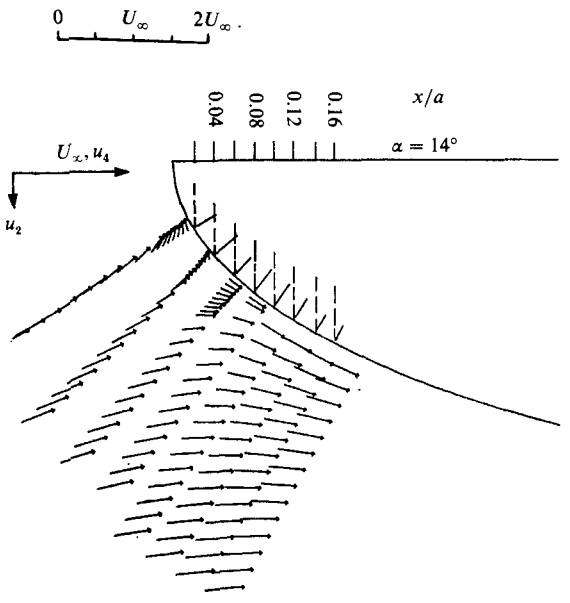

FIGURE 12. Steady velocity vectors at stagnation point.

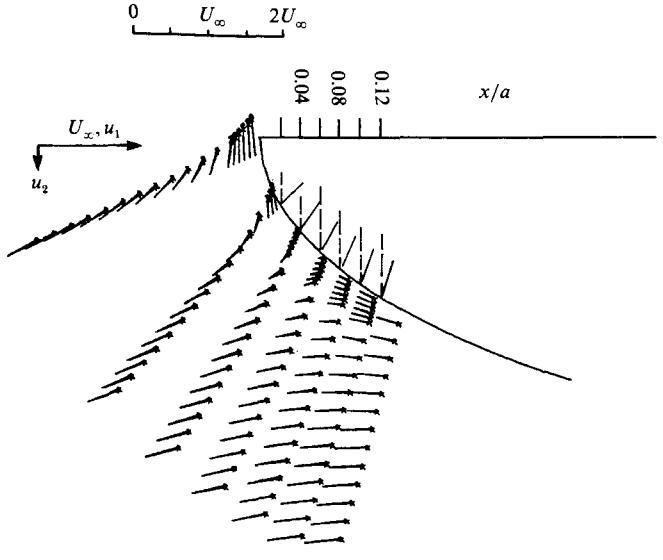

FIGURE 13. Unsteady velocity vectors at stagnation point. ×, $t = T$; △, $t = T/2$. (Owing to the scale chosen, it is necessary to display this information in one figure.)

4.4. *Pressure-side separation region*

In this region we obtained six steady and seven unsteady velocity profiles normal to the wall, at $x/a = 1.6$, 1.7, 1.75, 1.8, 1.85, 1.90, 1.95 (for the steady case the station $x/a = 1.9$ is not included). The unsteady velocity vectors are shown in figure 14. Typical time records are shown in figure 15 (station 5) together with time records

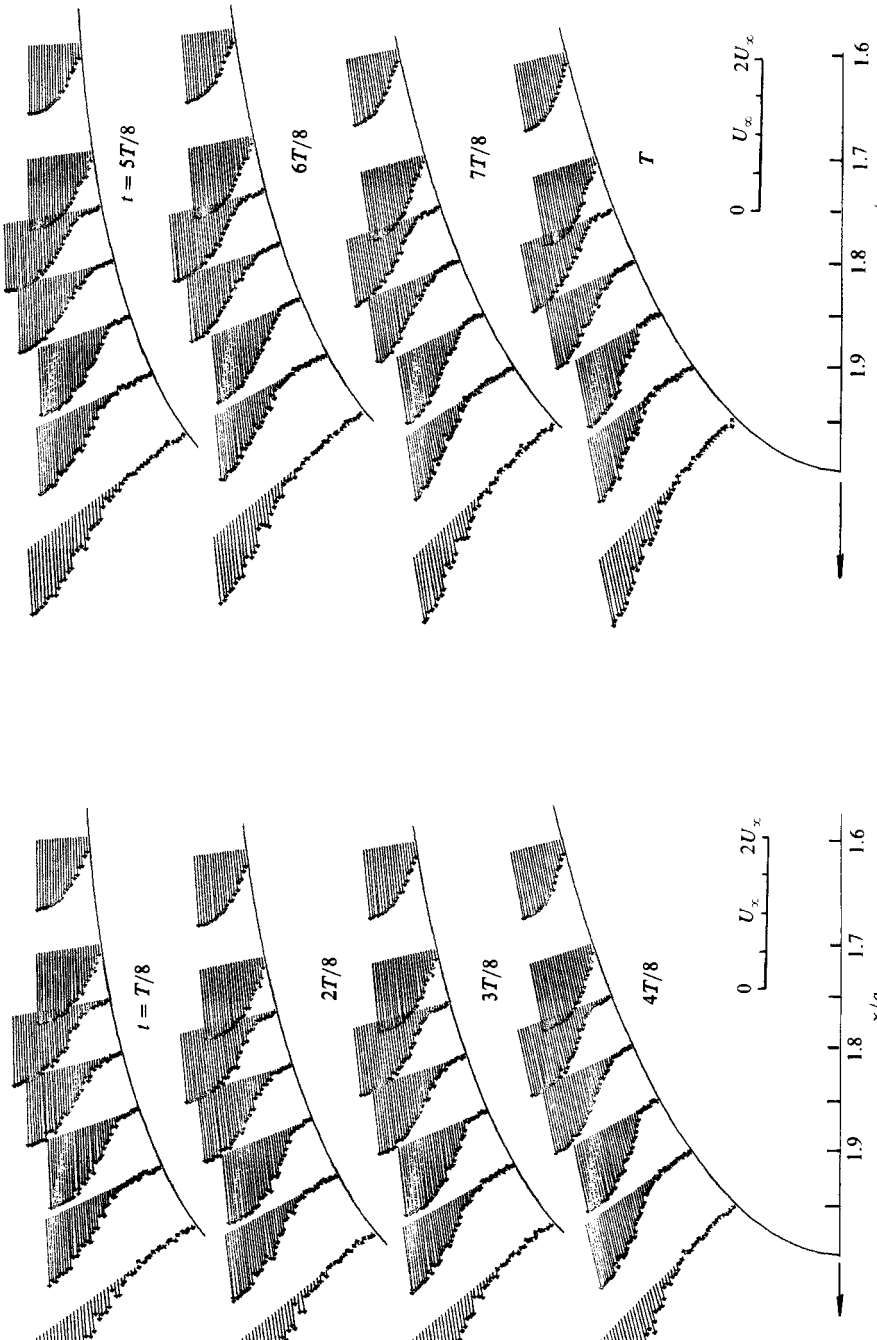

FIGURE 14. Velocity vectors at pressure-side separation region at eight instances within one period.

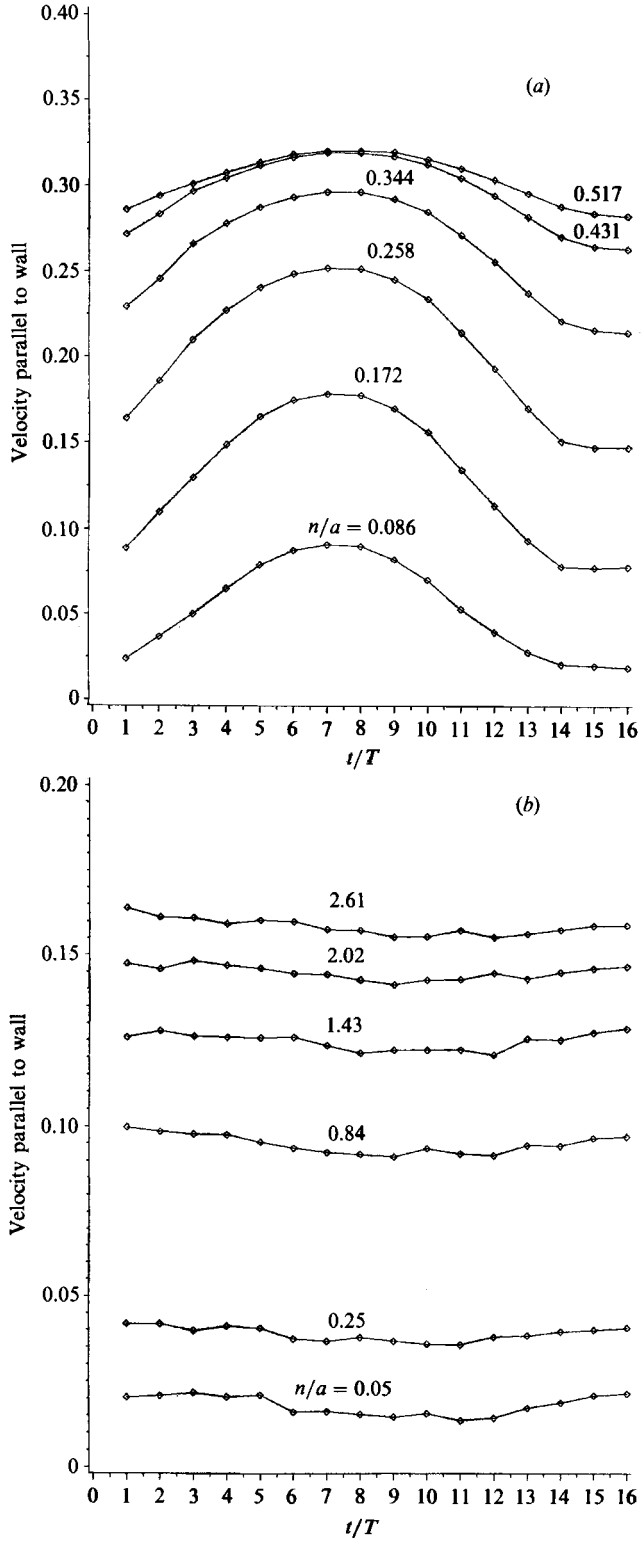

FIGURE 15. Time records of u-component at (a) suction-side separation region, and (b) pressure-side separation region, and at various locations away from the surface.

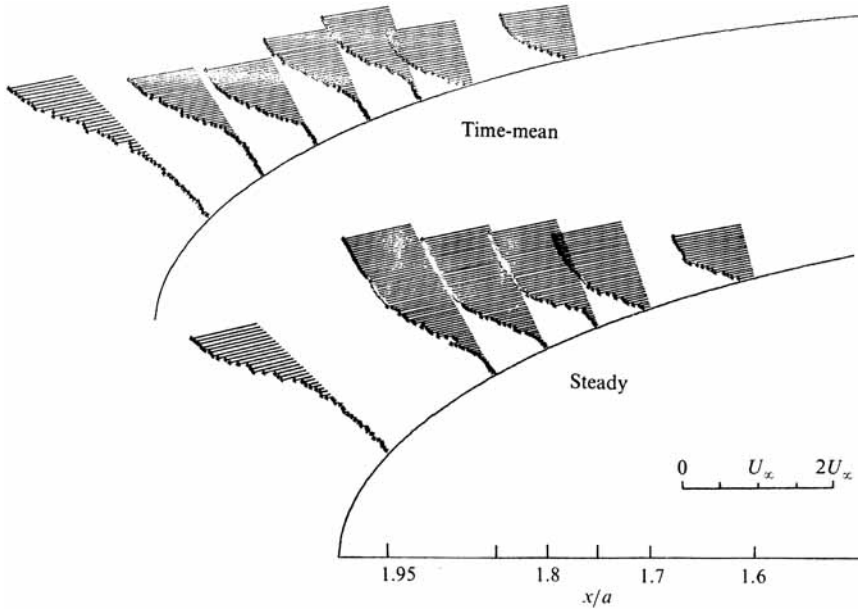

FIGURE 16. Steady and time-mean velocity vectors at pressure-side separation region.

from the suction-side separation region (station 3), for comparison. It appears that the motion of the suction-side free shear layer disturbs the flow on the pressure side, because the temporal variation of the velocity magnitude is not sinusoidal there. Moreover, our data (figure 7*b*) indicate that in this region the amplitudes are not as large as those in the suction-side separation region. In figure 16 we show the steady and unsteady time-mean velocity vectors for comparison.

The main conclusions we can draw from our data in this region are the following:

(*a*) the periodic character of the phenomenon in this region can barely be detected in the instantaneous frames. For all practical purposes we could argue that the flow is almost steady, only a little affected by the periodic pulsations of the free stream or the flapping of the free shear layer on the suction side of the body;

(*b*) the averaged unsteady vector profiles also differ marginally from their steady-flow counterparts.

4.5. *The wake*

Finally, measurements were taken in the wake in order to provide information about the shear layer emanating from the pressure-side separation point. The unsteady velocity vectors are shown in figure 17 and in figure 18 we show the steady and time-mean vectors. Here, the sinusoidal variation in time of the velocity is completely absent, because of the interaction of the two shear layers. The velocity profiles, as expected, tend to become uniform downstream of the trailing edge.

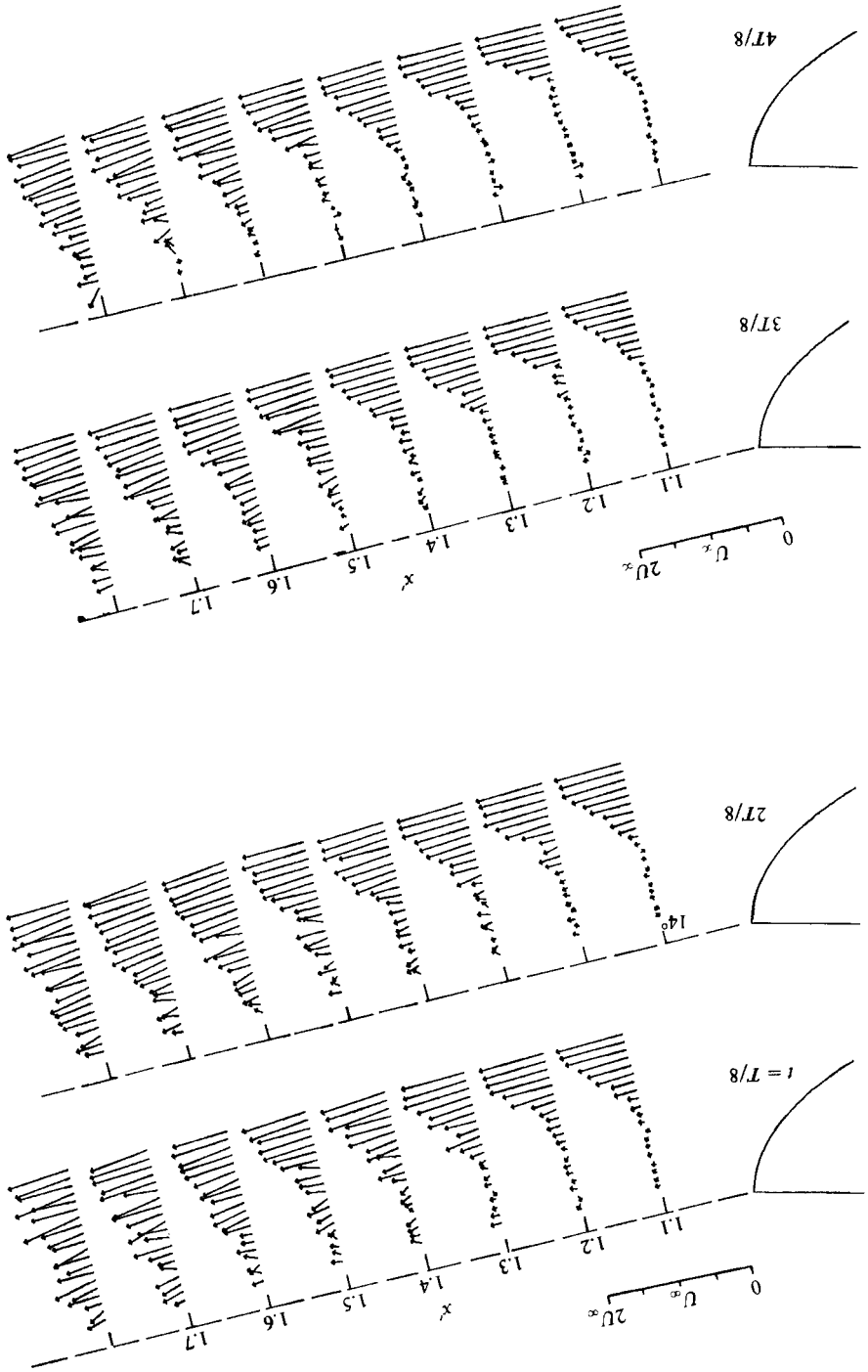

FIGURE 17. For caption see page 118.

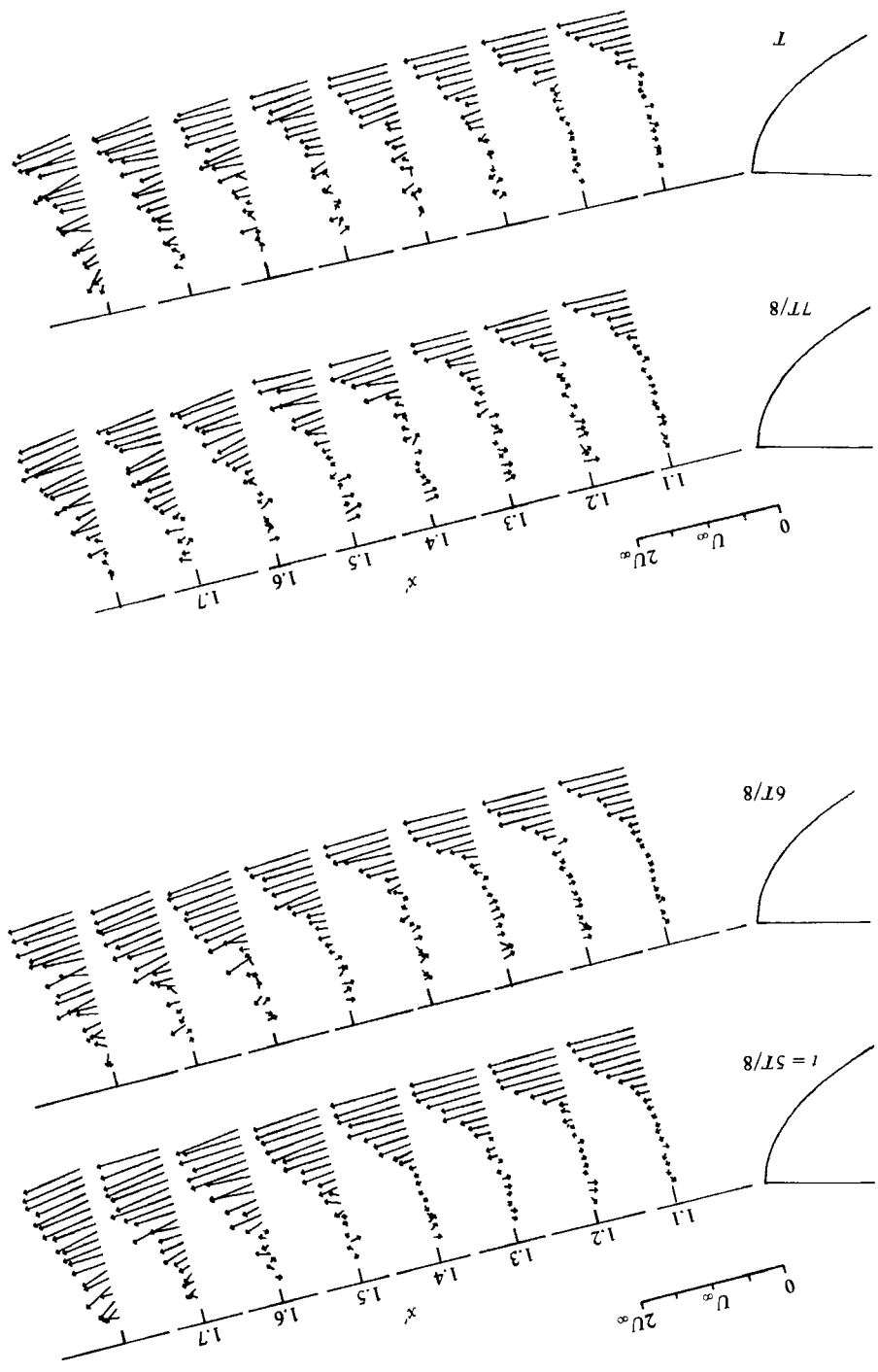

FIGURE 17. Velocity vectors in the wake at eight instances within one period.

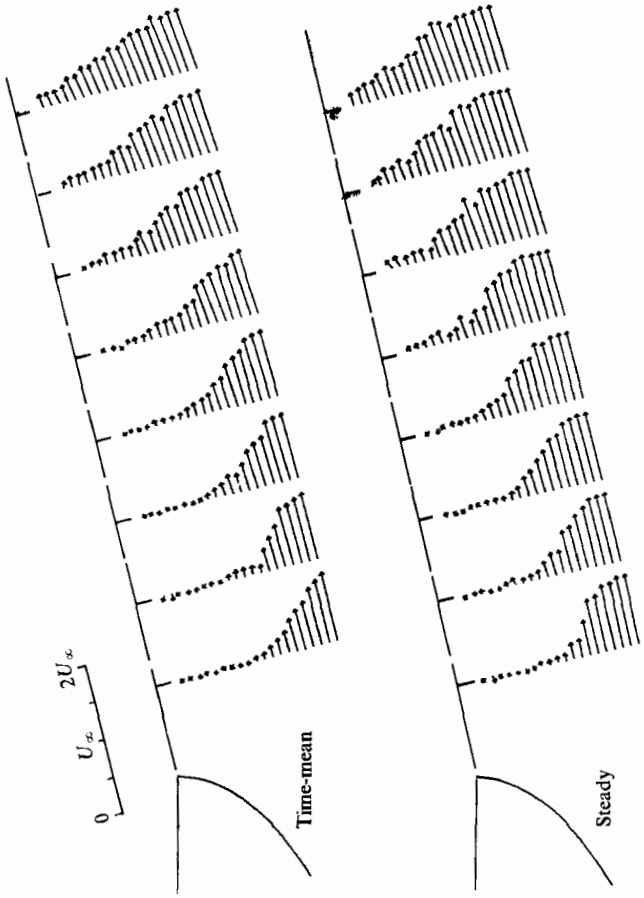

FIGURE 18. Steady and time-mean velocity vectors in the wake region.

5. Discussion and conclusions

The present experimental data present a comprehensive picture of the response of viscous periodic flow over a bluff body. Detailed phase-locked measurements allow the examination of events occurring in the stagnation region, in the separation regions, and in the free shear layers. Phase differences can thus be calculated.

A number of studies have examined the unsteady flow field over pitching airfoils, as reviewed extensively in McCroskey (1977). In the present study, the angle of attack is fixed and a disturbance is imposed only on the magnitude of the free stream. For this type of disturbance we found that the points of separation respond but their excursions are rather small. The excursions of the point of zero skin friction have an amplitude of approximately $a/10$ on the suction side but the corresponding quantity on the pressure side is almost negligible. In qualitative agreement with this observation, the inclination of the free shear layer on the suction side approaches the wall as separation moves downstream. The amplitude of the inclination of the free shear layer as defined approximately by the locus of the points of flow reversal is about 10°.

The stagnation point is also affected by the periodic disturbance in the free-stream magnitude. During acceleration and deceleration of the oncoming stream, stagnation is displayed towards the suction and pressure side respectively.

The natural frequency of vortex shedding in this problem is suppressed. In other words, the flow is locked on the external disturbance. Unlike the case of natural vortex shedding though, in the present case the points of separation move in phase downstream or upstream and as a result the width of the wake periodically increases and decreases.

We draw another interesting conclusion, based again on the topography of free shear layers, by comparing the steady to the time-mean field. Here the time-mean field is obtained by averaging information at a point along the entire period of oscillation. It appears that in the mean, both points of separation are displaced downstream and both free shear layers are forced closer to the body as compared to steady flow. The width of the wake and therefore drag should be decreased in the mean.

Unlike the separated regions studied by Francis *et al.* (1979) the wake studied here contains a permanently separated region. The term 'dead water' does not apply here because there is some activity beneath the free shear layers even at distances very close to the point of separation. However, the highly energetic flows observed by Francis *et al.* (1979) are not present.

This paper is dedicated to Professor W. R. Sears on the occasion of his 75th birthday.

This work was supported by U.S. Air Force Office of Scientific Research Grant No. 82-0228 and was monitored by Major Michael S. Francis.

REFERENCES

DESPARD, R. A. & MILLER, J. A. 1971 Separation in oscillating boundary-layer flows. *J. Fluid Mech.* **47**, 21–31.

DIDDEN, N. & HO, C.-M. 1985 Unsteady separation in oscillating boundary-layer flows. *J. Fluid Mech.* **160**, 235–256.

FRANCIS, M. S., KEESE, J. E., LANG, J. D., SPARKS, G. W. & SISSON, G. E. 1979 Aerodynamic characteristics of an unsteady separated flow. *AIAA J.* **17**, 1332–1339.

KOROMILAS, K. A. & TELIONIS, D. P. 1980 Unsteady laminar separation – an experimental study. *J. Fluid Mech.* **95**, 347–384.

MATHIOULAKIS, D. S. & TELIONIS, D. P. 1985 Velocity and vorticity measurements around laminar separation. In *Numerical and Physical Aspects of Aerodynamic Flows* (ed. T. Cebeci), pp. 7.3–7.12. Springer.

MATHIOULAKIS, D. S. & TELIONIS, D. P. 1987 Velocity and vorticity distributions in periodic separating flow. *J. Fluid Mech.* **184**, 303–333.

MCCROSKEY, W. J. 1977 Some current research in unsteady fluid dynamics – The 1976 Freeman Scholar Lecture. *Trans. ASME* I: *J. Fluids Engng* **99**, 8–38.

MESSITER, A. F. 1979 Boundary-layer separation. In *Proc. 8th U.S. Nat. Congr. Appl. Mech.*, pp. 157–179. North Hollywood: Western Periodicals.

MESSITER, A. F. 1983 Boundary-layer interaction theory. *J. appl. Mech.* **50**, 1104–1113.

MEZARIS, T. B., BARBI, C., JONES, G. S. & TELIONIS, D. P. 1987 Separation and wake of pulsating laminar flow. *Phil. Trans. R. Soc. Lond.* A **322**, 493–523.

MOORE, F. K. 1958 On the separation of the unsteady boundary layer. *Boundary Layer Research* (ed. H. Görtler), pp. 296–311. Springer.

ROTT, N. 1956 Unsteady viscous flow in the vicinity of a stagnation point. *Q. Appl. Maths* **13**, 444.

SEARS, W. R. 1956 Some recent developments in airfoil theory. *J. Aero. Sci.* **23**, 490–499.

SEARS, W. R. & TELIONIS, D. P. 1975 Boundary-layer separation in unsteady flow. *SIAM J. Appl. Maths* **28**, 215–235.

SHEN, S. F. 1978 Unsteady separation according to the boundary-layer equation. *Adv. Appl. Mech.* **18**, 177–220.

SMITH, F. T. 1977 The laminar separation of an incompressible fluid streaming past a smooth surface. *Proc. R. Soc. Lond.* A **356**, 433–463.

SMITH, F. T. 1979 Laminar flow of an incompressible fluid past a bluff body: the separation, reattachment, eddy properties and drag. *J. Fluid Mech.* **92**, 171–205.

SMITH, F. T. 1985*a* A structure for laminar flow past a bluff body at high Reynolds number. *J. Fluid Mech.* **155**, 175–191.

SMITH, F. T. 1985*b* Nonlinear effects and non-parallel flows; the collapse of separating motion. *United Tech. Research Center, E. Hartford, CT, Rep.* 85-55.

SMITH, F. T. 1986 Steady and unsteady boundary-layer separation. *Ann. Rev. Fluid Mech.* **18**, 197–220.

SYCHEV, VIK. V. 1979 Asymptotic theory of nonstationary separation. *Fluid Dyn.* **14**, 829–838.

TELIONIS, D. P. 1979 Review – unsteady boundary layers, separated and attached. *Trans. ASME* I: *J. Fluids Engng* **101**, 29–43.

TELIONIS, D. P. 1981 *Unsteady Viscous Flow.* Springer.

TELIONIS, D. P. & KOROMILAS, C. P. 1978 Flow visualization of transient and oscillatory separating laminar flows. In *Nonsteady Fluid Dynamics* (ed. D. E. Crow & J. A. Miller), pp. 421–32. ASME.

TELIONIS, D. P. & MATHIOULAKIS, D. S. 1984 On the shedding of vorticity at separation. In *Unsteady Separated Flows* (ed. M. W. Luttges), pp. 106–116. AFOSR, SRL/University of Colorado.